Solid State Ionics 359 (2021) 115534

Contents lists available at ScienceDirect

Solid State Ionics

journal homepage: www.elsevier.com/locate/ssi

Increasing the thermal expansion of proton conducting Y-doped $BaZrO_3$ by Sr and Ce substitution

Amir Masoud Dayaghi [a], Reidar Haugsrud [a], Marit Stange [b], Yngve Larring [b], Ragnar Strandbakke [a], Truls Norby [a,*]

[a] Department of Chemistry, Centre for Materials Science and Nanotechnology, University of Oslo, FERMiO, Gaustadalléen 21, NO-0349 Oslo, Norway
[b] SINTEF, POB 124 Blindern, NO-0314 Oslo, Norway

ARTICLE INFO

Keywords:
Barium zirconate
BZY
Thermal expansion coefficient
TEC
Conductivity
Proton
Proton ceramic electrochemical cells
Metal-supported

ABSTRACT

Proton conducting oxide electrolytes find potential application in proton ceramic fuel cells and electrolyzers operating at intermediate temperatures, e.g. 400–600 °C. However, state-of-the-art proton conducting ceramics based on Y-doped $BaZrO_3$ (BZY) have lower thermal expansion coefficient (TEC) than most commonly applied or conceived supporting electrode structures, making the assembly vulnerable to degradation due to cracks or spallation. We have increased the TEC of 20 mol% Y-doped BZY (BZY20) by partially substituting Ba and Zr with Sr and Ce, respectively, to levels which still maintain the cubic structure and sufficiently minor n-type conduction; $(Ba_{0.85}Sr_{0.15})(Zr_{0.7}Ce_{0.1}Y_{0.2})O_{2.9}$ (BSZCY151020). High temperature XRD shows that this material has a cubic structure (space group $Pm\bar{3}m$) in the temperature range of 25–1150 °C and a linear TEC of $\sim 10 \times 10^{-6}\ K^{-1}$, as compared to the $\sim 8 \times 10^{-6}\ K^{-1}$ for BZY. It exhibited a DC conductivity of ~5 mS cm^{-1} at 600 °C in wet H_2. This electrolyte with increased TEC may find application in proton ceramic electrochemical cells in general and metal supported ones in particular.

1. Introduction

State-of-the-art ceramic proton conducting electrolyte materials for electrochemical energy conversion cells based on Y-doped $BaZrO_3$ (BZY) exhibit lower thermal expansion coefficients (TECs) than most potential electrodes and metallic supports (Table 1). Such thermal mismatch can initiate cracking in the cell assembly and cause severe degradation [1]. A potential strategy is to increase the TEC by altering the electrolyte composition within the stability field of the cubic structure so as to keep the desired transport properties. $BaCeO_3$ and $SrZrO_3$ have higher TEC than $BaZrO_3$. They exhibit non-cubic structures depending on temperature [2–4], but the partial substitution of Ba and Zr in BZY by Sr and Ce, respectively, may still be possible within the stability field of the cubic structure while providing a significant increase in the TEC (Table 1) [3].

In the present contribution we demonstrate the feasibility of $(Ba_{0.85}Sr_{0.15})(Zr_{0.7}Ce_{0.1}Y_{0.2})O_{2.9}$ (BSZCY151020) as a new proton conducting oxide electrolyte with linear TEC more similar to potential electrodes and supports than traditional BZY electrolytes. BSZCY151020 and BSZCY151020 containing 1 wt% NiO as sintering aid were synthesized by solid state reaction sintering (SSRS) and the thermal expansion in dry atmospheres has been extracted from data produced by high temperature XRD. The electrical conductivity has been interpreted as a function of temperature and oxygen partial pressure in wet atmospheres.

2. Experimental

2.1. Materials synthesis

A mixture of precursor powders corresponding to a nominal composition $(Ba_{0.85}Sr_{0.15})(Zr_{0.7}Ce_{0.1}Y_{0.2})O_{2.9}$ (BSZCY151020) was prepared by ball milling $BaCO_3$ (99.9% purity, Sigma Aldrich, USA), $SrCO_3$ (99.9%, Sigma Aldrich), ZrO_2 (99.7% purity, Alfa Aesar, USA), CeO_2 (99.5% Alfa Aesar, USA), and Y_2O_3 (99.9% purity, Sigma Aldrich) using zirconia balls for 72 h in ethanol (absolute, VWR). One part of the powder was added 1 wt% NiO (99.9% Sigma Aldrich) and milled in a planetary ball mill for 1 h. The BSZCY151020 and BSZCY151020 + 1 wt % NiO powder mixtures were dried at 120 °C during stirring on top of hotplate, pressed uniaxially at 20 MPa into pellets and reaction sintered for different durations and temperatures; 12 h at 1550 °C for

* Corresponding author.
E-mail address: truls.norby@kjemi.uio.no (T. Norby).

https://doi.org/10.1016/j.ssi.2020.115534
Received 13 June 2020; Received in revised form 6 December 2020; Accepted 7 December 2020
Available online 16 December 2020

Table 1
Linear thermal expansion coefficient (TEC) of relevant undoped perovskites and acceptor-doped proton conducting perovskites, along with Y-stabilized ZrO_2 (YSZ) and stainless steel for comparison.

Materials	TEC (10^{-6} K^{-1})	Atmosphere	Temp. range (°C)	Ref.
$BaZrO_3$	7.13	Reducing	25–800	[5]
$BaCeO_3$	11.2	Reducing	25–800	[5]
$SrZrO_3$	9.7	–	25–800	[6]
$SrCeO_3$	11.1	–	25–800	[6]
$BaZr_{0.80}Y_{0.20}O_{3-d}$	8.2	Air	100–900	[7]
$BaZr_{0.60}Ce_{0.2}Y_{0.2}O_{3-d}$	9.1	Dry, wet	100–900	[7]
$BaZr_{0.1}Ce_{0.7}Y_{0.2}O_{3-d}$	10.1	Air	25–1000	[8]
YSZ	10.5	Air	30–800	[9]
Stainless steel 434 L	10.4	–	30–800	[10]

BSZCY151020 + 1 wt% NiO, 12 h at 1600 °C for BSZCY151020, and 48 h at 1650 °C for BSZCY151020. To reduce effects of Ba evaporation, the pellets were covered by $BaZ_{0.85}Y_{0.15}O_{3-d}$ powder (CerPoTech, Norway) during sintering, and the outer layer of the pellets was moreover removed by grinding.

2.2. Powder X-ray diffraction and morphology studies

X-ray diffraction (XRD, D/MAX 2500, Rigaku, USA) analyses of the BSZCY151020 pellets were performed for phase identification using Cu Kα radiation in the 2θ range 20°–90°. The morphological features of the prepared pellets were investigated by field-emission scanning electron microscopy (FE-SEM, S-4700, Hitachi High Tech, Japan).

2.3. High temperature (HT-)XRD studies

To determine the TEC of BSZCY151020 electrolytes from the temperature dependence of the unit cell axes, HT-XRD data were collected with a Bruker D8 A25 diffractometer in reflection mode, equipped with a Lynxeye XE detector for high energies, using Mo$K\alpha$ radiation and focusing mirror optics. Temperature was controlled by an Anton Paar HTK1200 furnace with an alumina flat plate sample holder under flowing nominally dry synthetic air. The HT-XRD was performed during cooling in the temperature range 1150–30 °C, between $2\theta = 8°$ and 40° in steps of $\Delta(2\theta) = 0.015°$; data collection time was 16 min. The temperature step was 50 °C for the temperature range 750–200 °C where hydration and dehydration takes place and 100 °C for other temperature ranges. Rietveld refinements were performed with TOPAS [11] using 6271 data points, 221 Bragg reflections, and a maximum of 21 variables. The background was modelled using a Chebyshev polynomial and peak shapes were modelled by the modified Thompson-Cox-Hastings pseudoVoigt function. The refinements were performed with R-pattern R_P of 4–7%, R-weighted pattern R_{wp} = 5–9%, and goodness-of-fit S = 1–3.

Linear TECs are determined from the HT-XRD data as $\frac{1}{a}\frac{da}{dT}$ where a is the lattice constant. They were fitted separately in the two temperature intervals 30–450 °C and 600–1150 °C representing, respectively, frozen-in small level of hydration from traces of water in the nominally dry air, and equilibrium fully dehydrated sample. The TEC and chemical expansion in the intermediate region are not evaluated here.

2.4. Electrical characterization

Pt ink (Metalor, 6926) was painted as electrodes on both sides of the BSZCY151020 pellets and dried at 90 °C for 15 min. Pt wires were pressed onto a Pt mesh and attached to the electrodes with another layer of Pt ink, and the assembly was fired at 800 °C for 2 h.

The pellets were mounted in a ProboStat™ (NORECS, Norway) sample holder with a 4-wire 2-electrode configuration, and the electrical conductivity was characterized with a Novocontrol Alpha A impedance spectrometer coupled with a POTGAL interface (Novocontrol Technologies, Germany). Impedance sweeps (1 MHz–0.01 Hz, 50 mV rms) were collected every 50 °C from 650 to 150 °C in wet 5% H_2 in Ar after equilibration at each temperature. For wetting, the gas was bubbled at room temperature through a first bubbler with pure H_2O and a second one with saturated KBr (aq), yielding approximately 2.6% (0.026 atm) H_2O. The conductivity was, moreover, measured as a function of the oxygen partial pressure at 650 °C by using pure O_2, Ar/air and Ar/H_2 gas mixtures at fixed water vapor pressure (0.026 atm). The impedance spectra were fitted using the ZView program [12] to equivalent circuit models consisting of resistors R and constant phase elements Q of the form $R_b(R_{gb}Q_{gb})(R_{e1}Q_{e1})(R_{e2}Q_{e2})$ for BSZCY151020 or $(R_bQ_b)(R_{gb}Q_{gb})(R_eQ_e)$ for BSZCY151020 + NiO. Subscripts b, gb and e/e1/e2 denote bulk, grain boundary and electrode contributions, respectively, assigned based on their capacitances. Bulk and grain boundaries had volume specific capacitances of the order of 10^{-12} and 10^{-9} F cm^{-1}, respectively, while area specific capacitances for electrodes were of the order of 10^{-6} F cm^{-2} (e and e1), and 10^{-4} F cm^{-2} (e2) [13]. The DC conductivity (σ) of the materials was calculated using the sum of bulk and grain boundary resistance, and the activation energies (E_a) for the conductivities were derived from an Arrhenius-type equation of the form:

$$\sigma = \frac{A}{T} exp\left(-\frac{E_a}{RT}\right) \quad (1)$$

where, A is a constant, R is the gas constant, and T is absolute temperature.

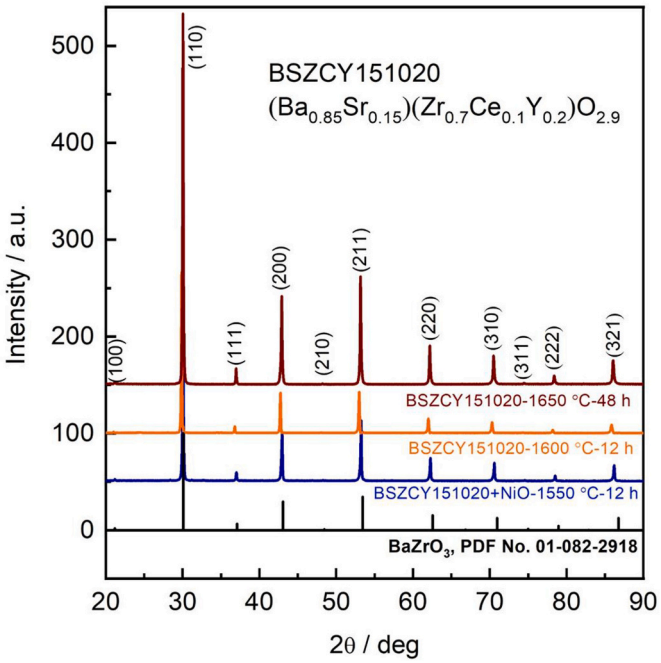

Fig. 1. XRD pattern of BSZCY151020 ($(Ba_{0.85}Sr_{0.15})(Zr_{0.7}Ce_{0.1}Y_{0.2})O_{2.9}$) and BSZCY151020 + NiO pellets synthesized by the solid state reaction (SSR) method at different temperatures and times. The PDF No. 01–082-2918 reference pattern is included.

3. Results and discussion

3.1. Structural and microstructural characterization

The X-ray diffraction (XRD) patterns of sintered BSZCY-NiO pellets are presented in Fig. 1. Single-phase specimens were obtained corresponding to the cubic $BaZrO_3$ perovskite phase. Upon sintering, the BSZCY151020 pellets remained white while the BSZCY151020-NiO

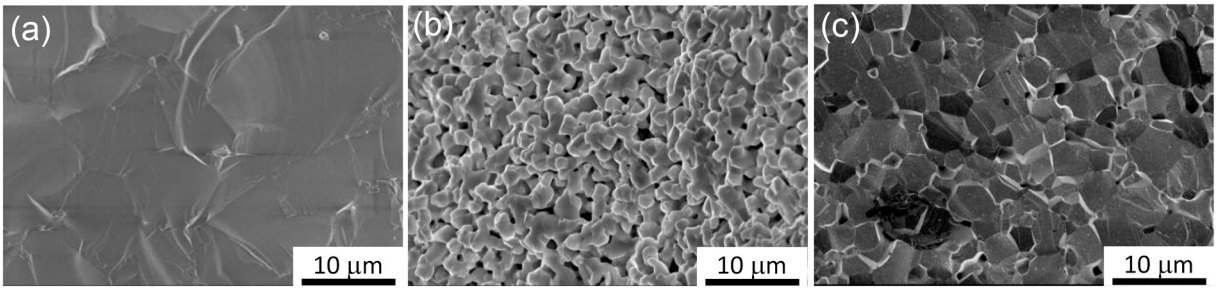

Fig. 2. Fracture cross-sections of (a) BSZCY151020 + NiO pellet with R.D. of 96% sintered at 1550 °C for 12 h, (b) BSZCY151020 pellet with R.D. of 57% sintered at 1600 °C for 12 h, and (c) BSZCY151020 pellet with R.D. of 92% sintered at 1650 °C for 48 h.

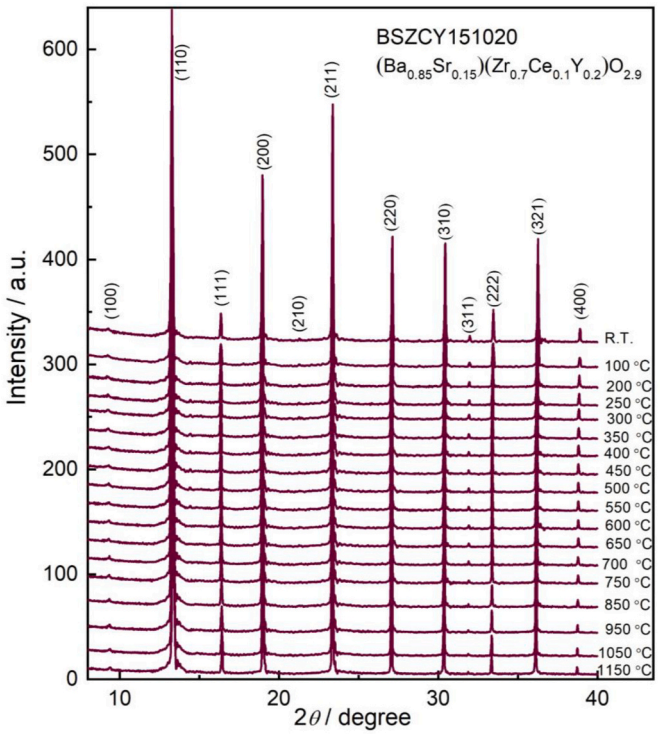

Fig. 3. XRD plot as a function of temperature of a BSZCY151020 pellet under cooling in the temperature range 1150–30 °C.

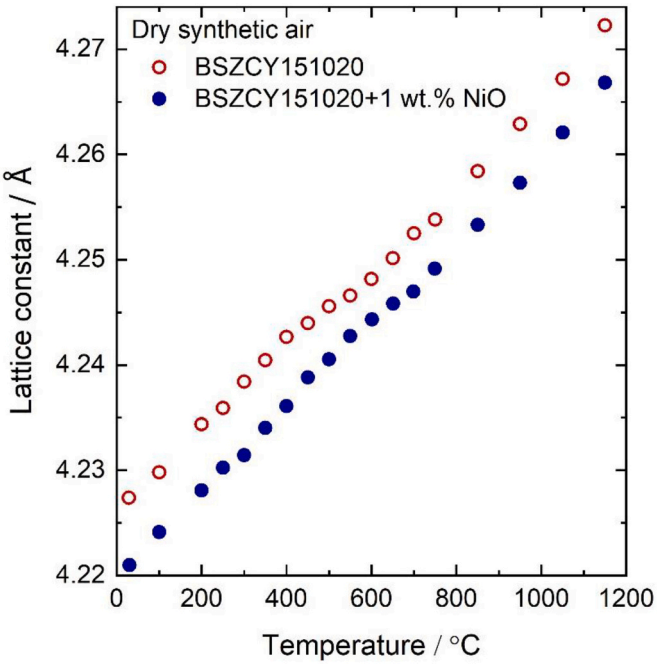

Fig. 4. Lattice constant of BSZCY151020 and BSZCY151020 + NiO as a function of temperature from HT-XRD during cooling in nominally dry synthetic air.

pellets became black. The lattice parameters of BSZCY151020 sintered at 1600 °C for 12 h and 1650 °C for 48 h are 4.2283 *Å* and 4.2280 *Å*, respectively, showing the negligible effect of sintering temperature and time. The lattice parameter of BSZCY151020 + NiO is 4.2211 *Å*, the difference to be discussed later.

Fig. 2 displays SEM micrographs of a fracture cross-section of the BSZCY151020 + NiO pellet sintered at 1550 °C (Fig. 2a) and BSZCY151020 pellets sintered at 1600 °C for 12 h (Fig. 2b) and 1650 °C for 48 h (Fig. 2c). The BSZCY151020 + NiO pellet showed a relative density (R.D.) as high as ~96% (determined by the Archimedes method). Without sintering aid, BSZCY151020 of 92% R.D. was obtained at the higher temperature (1650 °C) with prolonged sintering time (48 h). BSZCY151020 + NiO and BSZCY151020 pellets with R.D. higher than 90% were chosen for further HT-XRD and electrical characterization.

3.2. HT-XRD and TEC

XRD patterns of BSZCY151020 recorded during cooling in dry synthetic air are shown in Fig. 3. All the XRD patterns could be indexed according to the cubic $Pm\bar{3}m$ space group. A minor secondary phase reflection is seen at $2\theta \approx 14°$, especially below 600 °C, corresponding to the presence of some $BaCO_3$ probably with a content of Sr, precipitated on surfaces from and via grain boundaries [14]. This is in accord with the minor shoulders on the main peaks then reflecting outer regions of the grains being under-stoichiometric of Ba and Sr. This will hardly affect our calculated lattice parameters and TEC values much, as they are based on the main peaks reflecting the main phase of the presumably correctly composed interiors of the grains.

The lattice parameters for the BSZCY151020 and BSZCY151020 + NiO materials during cooling are displayed as a function of temperature in Fig. 4. The lattice parameter of BSZCY151020 at room temperature after cooling (4.2273 *Å*) is slightly lower than nominal $BaZ_{0.8}Y_{0.2}O_{3-d}$ (4.2292 *Å* [15]) which can be rationalized by the substitution of Ba ions with Sr ions: Sr^{2+} has a significantly smaller ionic radius than Ba^{2+} (1.18 vs 1.61 Å at 12-fold coordination). This presumably dominates the effect on the unit cell volume compared to that of the B-site substitution where Ce^{4+} has slightly higher radius than Zr^{4+} (0.87 vs 0.72 Å at 6-fold coordination) [16]. Furthermore, the perovskite lattice parameter for the BSZCY151020 + NiO (4.2209 *Å*) is slightly smaller than for BSZCY151020 without sintering aid, which may reflect some solubility of NiO in the perovskite lattice [17,18], and/or extraction of BaO from it [19].

Table 2
Linear TEC of BSZCY151020 and BSZCY151020 + NiO during cooling extracted from HT-XRD data (Fig. 4).

Material	$TEC_{(30–450\ °C)}$ (10^{-6} K^{-1})	$TEC_{(600–1150\ °C)}$ (10^{-6} K^{-1})	Remark
BSZCY151020	10.07 ± 0.03	10.11 ± 0.02	Synthetic air/ This study
BSZCY151020 + NiO	9.71 ± 0.01	9.73 ± 0.01	Synthetic air/ This study
BZY10	7.27	8.45	Dry air/ [21]
BZY10	7.29	7.13	Air+3% H_2O/ [21]
BZY15	8.0	8.0	Dry/ [23]

Table 2 summarizes the average linear TEC in the low (30–450 °C) and high (600–1150 °C) temperature region determined from the data in Fig. 4. In the intermediate temperature range 450–600 °C, the lattice parameter deviates from a linear temperature dependence, more pronounced for BSZCY151020 + NiO than BSZCY151020 materials. This reflects chemical expansion (CE) originating from effects of dehydration/hydration of oxygen vacancies in BZY materials [20,21]. Chemical expansion in the electrolyte in the dehydration/hydration region can cause delamination and micro-cracks unless attended to by suitable procedures during operational cycles [1,20–22], but is not the scope of the present work.

This new BSZCY151020 electrolyte has higher TEC than standard BZY formulations, e.g., $BaZr_{0.9}Y_{0.1}O_{3-d}$ (BZY10; Table 2) [21], showing the proof of concept for increasing the TEC with 15% Sr and 10% Ce being substituted for Ba and Zr, respectively, in BZY.

3.3. Electrical properties

The conductivities of BSZCY151020 and BSZCY151020 + NiO are derived from impedance spectroscopy. Representative Nyquist plots at high (600 °C) and low (200 °C) temperatures are shown for BSZCY sintered at 1650 °C for 48 h in Fig. 5a and b and for BSZCY151020 + NiO sintered at 1550 °C for 12 h in Fig. 5c and d. The impedance spectra have been interpreted according to the circuit models described earlier.

Fig. 6 reports the temperature dependence of the electrolyte DC conductivity (Fig. 6a) across the measured temperature window, and delineated bulk and grain boundary conductivities (Fig. 6b) in the low temperature region 300–150 °C in wet 5% H_2. The curve in Fig. 6a of the BSZCY151020 sample reflects the typical behavior of a material where the electrical conductivity is dominated by protons in the low temperature region and eventually levels off when the proton concentration decreases by dehydration at the highest temperatures [18,24].

The NiO containing sample exhibits lower conductivity and less levelling off at high temperatures. This reflects lower effective acceptor dopant level, fewer hydratable oxygen vacancies, hence fewer protons and lower proton conductivity of the hydrated material, and can via defect chemistry be shown to shift the dehydration to higher temperatures. At low temperatures where the concentration of protons can be assumed to be constant, the activation energy of the bulk conductivity evaluated from Eq. (1), representing the enthalpy of the charge mobility of protons, is ~49 kJ mol^{-1} for BSZCY151020 and ~ 65 kJ mol^{-1} for BSZCY151020 + NiO. These observations are in accordance with literature for comparable BZY materials [25].

The effect of NiO sintering aid to lower the content of effective acceptors, oxygen vacancies, and protons upon hydration, and to increase the activation energy and lower the level of proton conductivity, are well known [17,25,26]. It may be attributed to the effect the Ni^{2+} may have on the perovskite defect structure; 1 wt% NiO corresponds to as much as 3.7 mol% Ni^{2+}, which preferably dissolves interstitially, forming donors [17,25,26]. It is also known and recently emphasized that NiO extracts Ba from the perovskite precursors to form the low melting phase that promotes sintering, leaving the perovskite with Ba deficiency. This is then replaced by the intended acceptor dopant Y on Ba site, where it instead acts as a donor [19]. Reducing the negative effect of sintering aid NiO on the proton conductivity by adjusting the content and procedures of synthesis, fabrication, and sintering is important, but beyond the scope of the present study.

To show briefly the ionic versus electronic conduction, Fig. 7 displays the total electrical conductivity of the BSZCY151020 + NiO pellet versus oxygen pressure $p(O_2)$ at 650 °C under constant water vapor

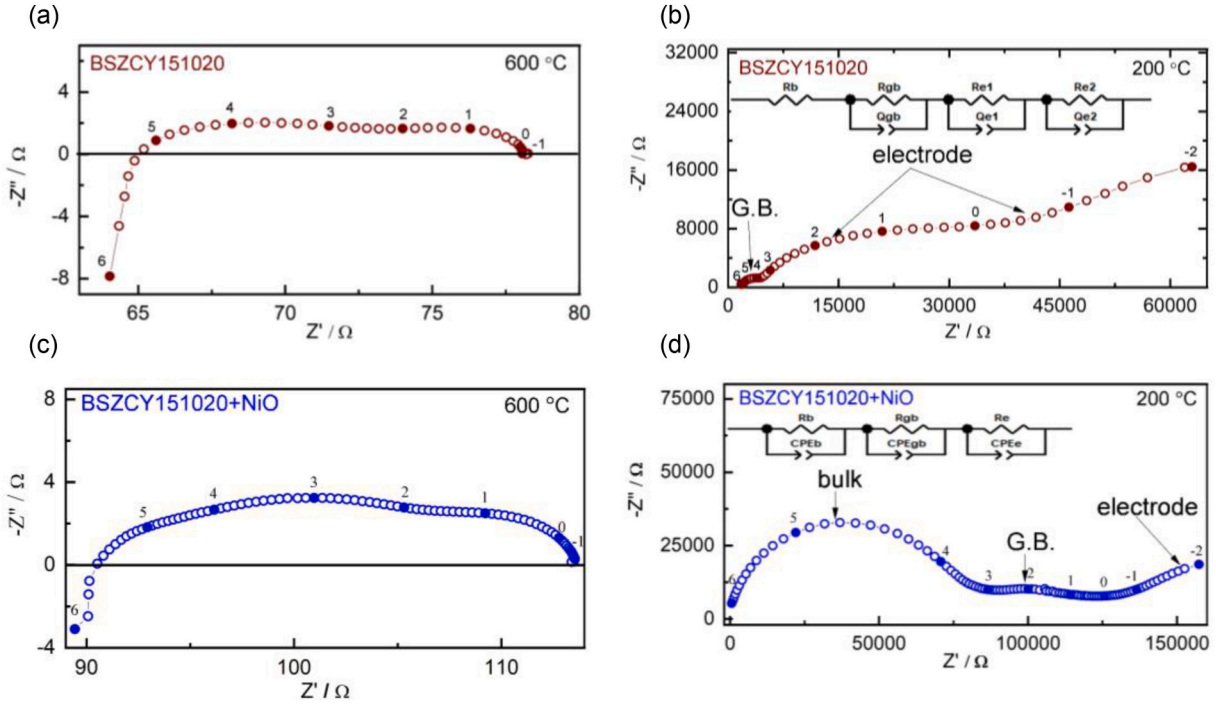

Fig. 5. Typical impedance spectra of (a and b) BSZCY151020 and (c and d) BSZCY151020 + NiO in wet 5% H_2 in Ar. The equivalent circuits are used for calculation of bulk (b) and grain boundary (G.B.) conductivities at low temperatures (300–150 °C). Numbers on the curves are log (frequency [Hz]).

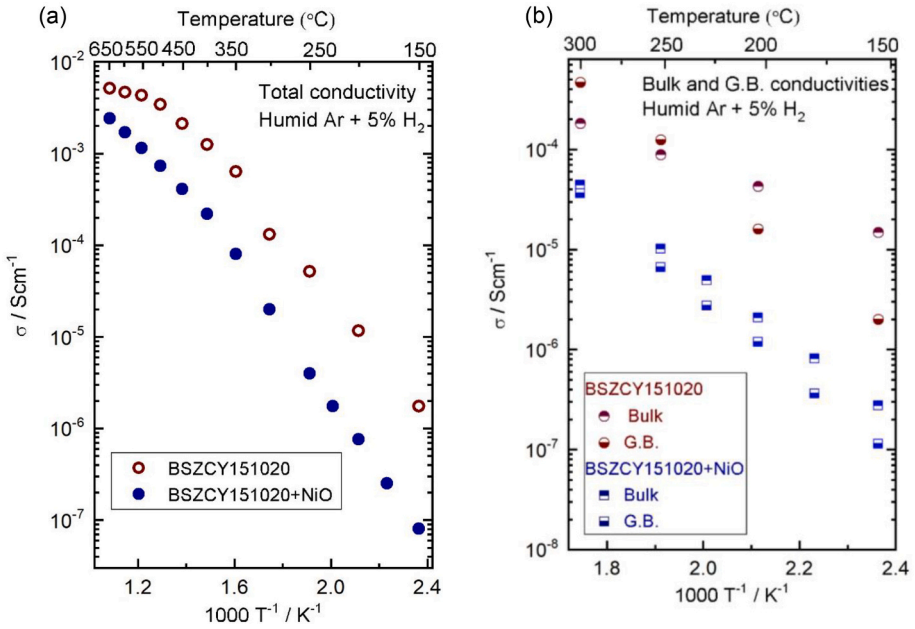

Fig. 6. Temperature dependence of electrical conductivity of BSZCY151020 and BSZCY151020 + NiO. (a) DC conductivity, (b) Bulk and grain boundary (G.B.) conductivities.

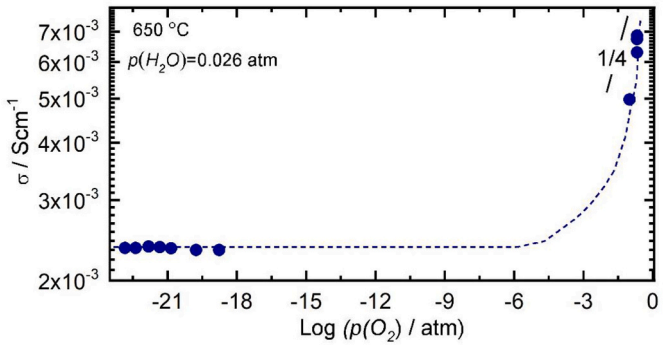

Fig. 7. DC conductivity vs. oxygen partial pressure in wet atmosphere at 650 °C for BSZCY151020 + NiO.

pressure. The plot resembles the literature of BZY showing predominance of $p(O_2)$ independent ionic conductivity at low $p(O_2)$ and an increase under oxidizing conditions approaching a $p(O_2)^{1/4}$ dependency due to an increasing contribution of p-type electronic conduction [13,15,26].

All in all, we have shown that the TEC can be increased by substituting Sr and Ce up to certain levels into BZY while the cubic structure and conductivity characteristics remained. The proton conductivity of BSZCY151020 and BSZCY151020 + NiO at 650 °C reaches ~5 and ~ 2 mS cm^{-1}, respectively, which is in the range of typically reported proton conductivities in BZY materials e.g., σ_{BZY20} ~ 3 mS cm^{-1} at 650 °C [27]. The new BSZCY151020 electrolyte can replace BZY for the fabrication of cermet supported and, in particular, metal-supported proton ceramic fuel cells and electrolyzers [28] with expectedly less problems with delamination and cracking due to TEC mismatch. Thin-film electrolytes of this composition can be applied using, for instance, pulsed laser deposition (PLD) or other methods onto the support, with functional porous intermediate layers based on Ni cermets, donor doped $SrTiO_3$, etc. BSZCY151020 has similar linear TEC as donor-doped $SrTiO_3$ (10.35×10^{-6} K^{-1} [29]) and ferritic stainless steel (10.4×10^{-6} K^{-1} [10]). According to the proton conductivities in Fig. 6, the area-specific resistance (ASR) of a 2 μm BSZCY151020 electrolyte will be ~40 mΩ cm^2 at 600 °C in wet atmospheres.

4. Conclusions

We report a new proton-conducting electrolyte, $(Ba_{0.85}Sr_{0.15})(Zr_{0.7}Ce_{0.1}Y_{0.2})O_{2.9}$, with increased linear TEC ~10×10^{-6} K^{-1}, and hence less TEC mismatch with the other cell components. HT-XRD showed that the cubic structure of the material was preserved at all temperatures in the range 30–1150 °C. NiO addition reduces the sintering time and temperature, but leads to a reduction of proton bulk and grain boundary conductivities. The proton conductivity of BSZCY151020 without NiO sintering aid reaches ~5 mS cm^{-1} at 600 °C, therefore it can be used in thin films as proton-conducting electrolyte.

Ethical statement

The authors consciously assure that for the manuscript "Increasing the thermal expansion of proton conducting Y-doped BaZrO3 by Sr and Ce substitution" the following is fulfilled: This material is the authors' own original work, which has not been previously published elsewhere. The paper reflects the authors' own research and analysis in a truthful and complete manner. The paper properly credits the meaningful contributions of co-authors and co-researchers. The results are appropriately placed in the context of prior and existing research. All sources used are properly disclosed All authors have been personally and actively involved in substantial work leading to the paper, and will take public responsibility for its content. http://www.elsevier.com/editors/plagdetect We agree with the above statements and declare that this submission follows the policies of Solid State Ionics as outlined in the Guide for Authors and in the Ethical Statement.

Declaration of Competing Interest

The authors declare that they have no known competing financial interests or personal relationships that could have appeared to influence the work reported in this paper.

Acknowledgements

Financial support from the Research Council of Norway (RCN) through the ENERGIX project "AH2A" No: 268010 and EIG CONCERT project "DAICHI" No: 284289 is gratefully acknowledged.

References

[1] S. Wang, F. Zhao, L. Zhang, F. Chen, Solid State Ionics 213 (2012) 29.
[2] T. Sugimoto, S. Hasegawa, T. Hashimoto, Thermochim. Acta 530 (2012) 58.
[3] B. Kennedy, C. Howard, G. Thorogood, J. Hester, J. Solid State Chem. 161 (1) (2001) 106.
[4] K. Knight, Solid State Ionics 145 (1–4) (2001) 275.
[5] S. Yamanaka, M. Fujikane, T. Hamaguchi, H. Muta, T. Oyama, T. Matsuda, S.-i. Kobayashi, K. Kurosaki, J. Alloys Compd. 359 (1) (2003) 109.
[6] J.R. Tolchard, T. Grande, Solid State Ionics 178 (7) (2007) 593.
[7] Y.G. Lyagaeva, D. Medvedev, A. Demin, P. Tsiakaras, O. Reznitskikh, Phys. Solid State 57 (2) (2015) 285.
[8] Z. Zhu, J. Qian, Z. Wang, J. Dang, W. Liu, J. Alloys Compd. 581 (Supplement C) (2013) 832.
[9] F. Tietz, Ionics 5 (1–2) (1999) 129.
[10] A.M. Dayaghi, K.J. Kim, S.J. Kim, S. Kim, H. Bae, G.M. Choi, J. Power Sources 354 (2017) 74.
[11] A.A. Coelho TOPAS Academic V4 Coelho Software, Brisbane, Australia, 2005.
[12] D. Johnson, ZView: A Software Program for IES Analysis. Version 2.8, Scribner Associates, Inc, Southern Pines, NC, 2008.
[13] F. Iguchi, N. Sata, T. Tsurui, H. Yugami, Solid State Ionics 178 (7–10) (2007) 691.
[14] R. Sažinas, M.-A. Einarsrud, T. Grande, J. Mater, Chem. A 5 (12) (2017) 5846.
[15] S. Tao, J.T. Irvine, J. Solid State Chem. 180 (12) (2007) 3493.
[16] R.D. Shannon, Acta Crystallogr. A: crystal physics, diffraction, theoretical and general crystallography 32 (5) (1976) 751.
[17] J.M. Polfus, M.-L. Fontaine, A. Thøgersen, M. Riktor, T. Norby, R. Bredesen, J. Mater. Chem. A 4 (21) (2016) 8105.
[18] J. Tong, D. Clark, M. Hoban, R. O'Hayre, Solid State Ionics 181 (11−12) (2010) 496.
[19] Y. Huang, R. Merkle, J. Maier, Solid State Ionics 347 (2020) 115256.
[20] A.K. Andersson, S.M. Selbach, C.S. Knee, T. Grande, J. Am. Ceram. Soc. 97 (8) (2014) 2654.
[21] G. Hudish, A. Manerbino, W.G. Coors, S. Ricote, J. Am. Ceram. Soc. 101 (3) (2018) 1298.
[22] S. Yamaguchi, N. Yamada, Solid State Ionics 162 (2003) 23.
[23] K. Kreuer, Annu. Rev. Mater. Res. 33 (1) (2003) 333.
[24] Y. Yamazaki, R. Hernandez-Sanchez, S.M. Haile, Chem. Mater. 21 (13) (2009) 2755.
[25] S. Duval, P. Holtappels, U. Stimming, T. Graule, Solid State Ionics 179 (21–26) (2008) 1112.
[26] K.-Y. Park, Y. Seo, K.B. Kim, S.-J. Song, B. Park, J.-Y. Park, J. Alloys Compd. 639 (2015) 435.
[27] E. Fabbri, A. D'Epifanio, E. Di Bartolomeo, S. Licoccia, E. Traversa, Solid State Ionics 179 (15–16) (2008) 558.
[28] E. Stefan, M. Stange, C. Denonville, Y. Larring, N. Hildenbrand, T. Norby, R. Haugsrud, J. Mater. Sci. 52 (11) (2017) 6486.
[29] D. Neagu, J.T. Irvine, Chem. Mater. 22 (17) (2010) 5042.